On the assessment of the pressure coefficient on the mixed ventilation modeling

Marcos Batistella Lopes*[1], Gaëlle Guyot[2,3], and Nathan Mendes[1]

1 Pontifical Catholic University of Paraná
R. Imaculada Conceição, 1155
80.215-901, Curitiba (Paraná), Brazil
**Corresponding author: batistella.marcos@pucpr. br*

2 University of Savoie Mont Blanc
Boulevard du Lac, LOCIE
73.370 Le Bourget du Lac, France

3 CEREMA
46 Rue Saint-Théobald
38080 L'Isle-d'Abeau, France

ABSTRACT

The accurate estimation of the local wind pressure coefficient is crucial in the numerical modeling of natural or mixed ventilation in buildings subjected to wind. Building ventilation modeling typically relies on average wind pressure coefficient values specific to the building façade and wind direction. While the literature provides some correlations and standards for building wall-average pressure coefficients, these values are only useful in the absence of additional information or a database, as they can vary significantly based on urban forms. Field measurements, wind tunnel tests, and numerical modeling are the available methods for estimating pressure on building facades. In the first part of this study, the wall-average pressure coefficient was validated using Computational Fluid Dynamics (CFD) for both an isolated low-rise building and a non-isolated low-rise building. Acceptable relative errors were achieved for the non-isolated building in all wind directions. However, higher relative errors were observed for the non-isolated building at surface directions of 90° and 180° for wind directions exceeding 75°. In the second part of this study, a Building Energy Simulation Test was conducted to assess the impact of the pressure coefficient on ventilation modeling, comparing five scenarios: no wind action, standard pressure coefficient, literature correlation pressure coefficient, and CFD-derived pressure coefficient for isolated and non-isolated buildings. The results indicated relative differences on the order of 7% and 6% for Air Change Rate and CO_2 average concentrations, respectively. This research contributes to the understanding of performance indicators for Indoor Air Quality (IAQ) studies, emphasizing the importance of considering both intentional and involuntary airflows in ventilation design.

KEYWORDS

Pressure coefficient. Ventilation. CFD. IAQ. Multizone model.

1 INTRODUCTION

Thermal comfort and Indoor Air Quality (IAQ) are closely tied to effective ventilation and infiltration management, which directly impact a building's energy consumption. Ventilation encompasses intentional indoor air exchange, which can occur through natural means such as opening windows and doors, or through mechanical systems involving supply and exhaust fans (ASHRAE, 2021). On the other hand, infiltration refers to the unintentional flow of outdoor air into a building through unintended openings like cracks, gaps around windows, doors, and electrical components. Conversely, when this unintentional airflow exits the indoor space, it is termed exfiltration. Both infiltration and exfiltration contribute to air leakage, representing unintentional airflows within a building.

Natural ventilation and air leakage are influenced by pressure differentials across the building envelope, which can arise from various factors such as wind, stack effect, and ventilation fans.

In the case of natural ventilation, these pressure differentials are primarily generated by external forces like wind or temperature differences. In contrast, mechanical ventilation relies on devices such as supply and exhaust fans to create pressure differences and induce airflow. In real-world scenarios, buildings experience a combination of these driving forces simultaneously, and the resulting airflow through the building envelope is a culmination of their combined effects.

To accurately comprehend the driven mechanisms of wind and stack effects, it is crucial to gain a comprehensive understanding of the airflow patterns around the building. In the case of an isolated rectangular flat-roofed building, the mean wind flow pattern reveals intricate characteristics, including the presence of horseshoe vortices, corner streams, areas of flow separation and reattachment, as well as slow rotating vortices formed behind the building due to backflow (Oke et al., 2017). The flow in the immediate wake of the building and the stagnation points upstream and downstream of the wind direction further contribute to the complexity of the airflow. Additionally, the actual airflow around buildings includes a wide range of wind speeds and directions, showcasing distinctive transient features such as the formation and dissipation of separation and recirculation bubbles, as well as periodic shedding of vortices in the wake.

The assessment and understanding of the wind load on a building can be achieved through wind tunnel tests and/or Computational Fluid Dynamics (CFD) modeling (Picozzi et al., 2022). The complex airflow surrounding buildings includes various spatial and temporal scales, and accurately representing full-scale buildings requires satisfying specific similarity criteria. These criteria include geometric, dynamic, and kinematic similarities, as outlined by Shu et al. (2020).

The complexity of CFD codes arises from their requirement to solve a set of nonlinear partial differential equations called the Navier-Stokes equations (Ferziger et al., 2020). Furthermore, the airflow around buildings typically exhibits turbulence, necessitating the modeling of turbulence closure problem (Wilcox, 2006). These turbulence models require significant computational resources and many of them are impractical for building-related problems that rely on transient boundary conditions derived from weather files.

Numerical simulations are utilized for evaluating IAQ performance indicators. Accurate modeling necessitates considering the building interior, exterior environment, and building envelope (Beausoleil-Morrison, 2021). Achieving highly accurate building modeling involves using a combination of toolboxes rather than relying on a single software, a practice known as co-simulation or coupling. In recent years, several coupling approaches have been developed, mostly aimed at assessing building energy consumption by correcting the convection heat transfer coefficient, as highlighted in Singh and Sharston (2021). However, incorporating building ventilation and infiltration into IAQ remains a challenging task, resulting in only a limited number of studies in the literature that explore IAQ and CFD coupling approaches (Kato, 2018).

Wang et al. (2010) conducted CFD simulations to predict outdoor CO concentrations in a two-story home, where the primary source was a generator located near the house. They investigated the impact of varying the distance between the source and the house. Nikolaou and Michaelides (2016) studied two indoor environments by performing CFD simulations to analyse CO transport and determine the optimal quantity and location of CO concentration sensors for occupant safety. Argyropoulos et al. (2017) employed CFD-IAQ coupling to investigate building ingress, utilizing three models to calculate pressure coefficients, and applied them to two case studies. Szczepanik-Scislo (2022) utilized the CFD-IAQ approach to study the release of CO from an indoor gas furnace, modifying the geometry of an air terminal device to improve IAQ.

For the present study, the CFD code “CFD0 Editor” developed by Wang (2007) was employed. It is a plugin for Contam® (Dols and Polidoro, 2020), a software used for whole-building multizone airflow and contaminant transport analysis. Consequently, the first part of this study aims to enhance wall-averaged pressure coefficient profiles by employing CFD0-Contam indirect coupling (Wang et al., 2010). In the second part, the geometry from the Building Energy Simulation Test (BESTEST) MZ320 (Neymark and Judkoff, 2008) was selected, and boundary conditions were modified to assess the influence of wall-averaged pressure coefficients on certain IAQ indicators.

2 MODEL DESCRIPTION

2.1 Multizone model

Contam® operates on the basis of a multizone airflow network model. This model assumes well-mixed conditions within each zone, where air momentum effects, pressure, and species concentration are uniformly and homogeneously distributed. Furthermore, there is no integration with Building Energy Simulation (BES) software in this study, resulting in a constant temperature assumption. The contaminant flow balance is mathematically represented by:

$$\frac{\mathrm{dm}^{\alpha}_{\mathrm{cont},i}}{\mathrm{dt}} = \sum\nolimits_j \dot{\mathrm{m}}_{\mathrm{air},j\rightarrow i}\left(1-\eta^{\alpha}_j\right)\mathrm{C}^{\alpha}_j + \mathrm{G}^{\alpha}_i + \mathrm{m}_{\mathrm{air},i}\sum\nolimits_{\beta}\mathrm{K}^{\alpha,\beta}_i\mathrm{C}^{\beta}_i - \sum\nolimits_j \dot{\mathrm{m}}_{\mathrm{air},i\rightarrow j}\mathrm{C}^{\alpha}_i - \mathrm{R}^{\alpha}_i\mathrm{C}^{\alpha}_i \tag{1}$$

where $\mathrm{m}^{\alpha}_{\mathrm{cont},i}$ is the mass of a contaminant α in zone i, $\dot{\mathrm{m}}_{\mathrm{air},j\rightarrow i}$ is the rate of air mass flow from zone j to zone i, η^{α}_j is the filter efficiency of the contaminant α through the path between zones j and i, C^{α}_j is the concentration of contaminant α in the zone j, G^{α}_i is the α contaminant generation rate, $\mathrm{m}_{\mathrm{air},i}$ is the air mass in zone i, $\mathrm{K}^{\alpha,\beta}_i$ is the kinetic reaction coefficient in zone i between species α and β, C^{β}_i is the concentration of the component β in zone i, $\dot{\mathrm{m}}_{\mathrm{air},i\rightarrow j}$ is the rate of air mass flow from the zone i to the zone j, C^{α}_i is the concentration of contaminant α in zone i, and R^{α}_i is the removal coefficient of the component α in zone i.

To discretize the mass balance equation (Equation (1)), a control volume model employing the standard implicit method is employed. The resulting set of discretized equations is solved using both an iterative biconjugate gradient (BCG) algorithm and an iterative successive over-relaxation (SOR) algorithm, as described in Dols and Polidoro (2020).

2.2 CFD model

CFD codes are capable of handling non-uniformities and heterogeneities in fluid flow, although at a significant computational cost when dealing with multizone models. The mass and momentum equations for steady-state fluid flow can be expressed in the following general form, as shown in:

$$\nabla\cdot\left(\rho\mathbf{u}\varphi\right) - \Gamma_{\varphi}\nabla\cdot\left(\nabla\varphi\right) = S_{\varphi} \tag{2}$$

where ρ is the air density, **u** is the air velocity, φ is the transported property (mass or a velocity component), Γ_{φ} is the generalized diffusion coefficient, and S_{φ} is a source or sink term.

In certain simplified cases, such as some laminar flows, analytical solutions for the set of partial differential equations described in Equation (2) exist. However, for most flow problems, including airflow around bluff bodies, empirical and/or numerical solutions are necessary. Among the various numerical discretization methods available, the Finite Volume Method (FVM) is commonly employed. This method discretizes the domain into smaller control volumes and integrates the transport equations for each volume. To solve the convective, diffusive, and gradient terms arising from the FVM, numerical schemes are utilized. Additionally, addressing the turbulence closure problem requires numerical modeling, such as the Reynolds-Averaged Navier-Stokes (RANS) methods, which involve modeling eddies of all sizes through the Reynolds decomposition.

For dealing with incompressible airflow, the "CFD0 Editor" from Contam® comes into play. This software implements the Semi-Implicit Method for Pressure Linked Equations (SIMPLER) algorithm to determine the airflow field (Patankar, 1980). The liner eddy-viscosity model standard k-ε (Launder and Spalding, 1974) is employed as the High-Reynolds number turbulence model. Lastly, the convective terms are discretized using the power-law scheme.

2.3 Numerical Procedure

In the first part of this study, a validation study was conducted using two low-rise building geometries from the comprehensive wind pressure database of the School of Architecture & Wind Engineering at Tokyo Polytechnic University ("TPU Aerodynamic Database", 2023). The first building, considered in isolation, has dimensions of 4m × 16m × 40m, while the second building, non-isolated, has dimensions of 12m × 16m × 24m, with a plan density area of 0.2 and a canyon street aspect ratio of 1.0.

Following the grid refinement factors suggested by Blocken (2015), a grid convergence study was performed with three different grid resolutions. For the isolated building, the final grid consisted of 94 × 146 × 46 nodes, while the non-isolated building grid comprised 166 × 200 × 30 nodes. A length scale of 1:100 was applied, and the wind velocity at the height of the building was set to 7m/s.

The CFD study incorporated specific boundary conditions. The ground boundary was modeled as no-slip, the top of the computational domain was set as a slip wall, and the sides of the domain were designed as openings with an atmospheric boundary layer profile that varied with the wind direction. Figure 1 illustrates a top view of these grids, where H represents the height, W represents the width, and L represents the length of the building.

Figure 1: Mesh

(a) Isolated building. (b) Non-isolated building.

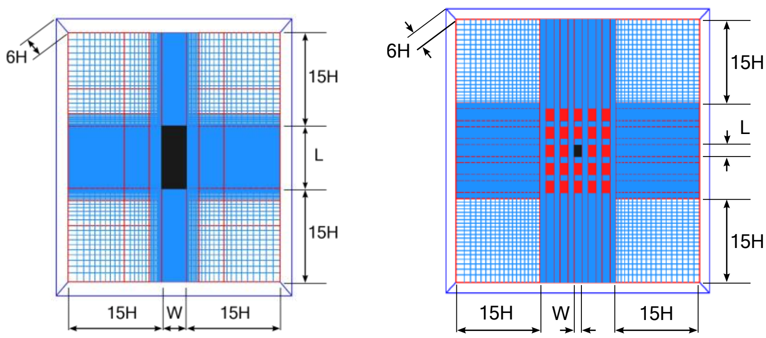

The local wind pressure coefficient is defined by:

$$C_{p,i} = \frac{P_i - P_\infty}{\frac{1}{2}\rho_\infty U_\infty^{\ 2}} \tag{3}$$

where ρ_∞ is the outdoor air density, U_∞ is the approach wind speed at upwind wall height, P_∞ is the local outdoor atmospheric pressure, and P_i is the pressure in a point i for a given wall surface under wind action.

Equation (3) provides a straightforward definition, but calculating the wind pressure coefficient is a complex task due to its dependence on factors such as the building shape, wind direction, and surrounding environment. To capture an accurate representation of the wall-averaged pressure coefficient for the building facades, this study employed a wind direction increment of 15° and 22.5°.

In the second part of this study, a test was conducted using the geometry depicted in Figure 2a, featuring three distinct zones: A, B, and C. Each zone shared the same dimensions of 8.0m × 6.0m × 2.7m. Zone C was equipped with an exhaust ventilation system operating at a rate of 1 Air Change per Hour (ACH), equivalent to approximately 130 m^3/h or 77 cubic feet per minute (cfm). Zone B had a constant emission rate of CO_2 at 18 l/h (Poirier et al., 2021) and followed a daily schedule from 5 pm to 9 am. The air leakage between zones was modeled using the power-law model based on Poirier (2023).

For the Contam® simulation (Figure 2b), the weather file for Lyon, France, was utilized, along with a constant outdoor CO_2 concentration of 400 ppm. The simulation spanned a week, starting from January 1st at 0h and concluding on January 7th at 24h, with a time step of 60 seconds.

Figure 2: Modified BESTEST MZ320

(a) Geometry of the BESTEST MZ320 (b) Contam® plan

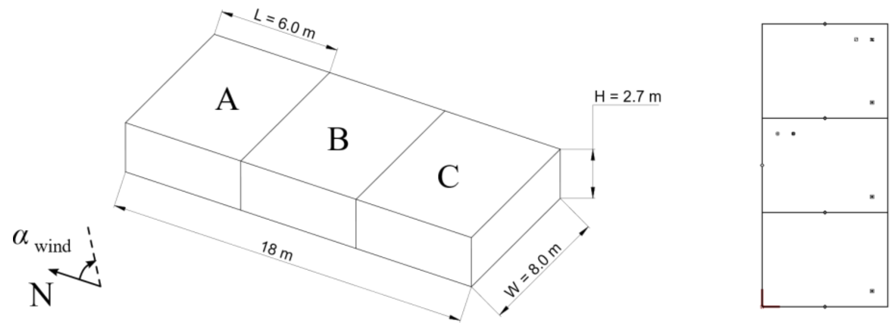

Table 1 presents the five different scenarios considered for the analysis of IAQ. The "No wind" case serves as the base case, focusing solely on mechanical ventilation, while the remaining cases involve mixed ventilation resulting from wind effects. According to the EN15242 regulation, windward facades are assigned a pressure coefficient of +0.5, while leeward facades receive a coefficient of -0.7 when no barriers are present.

Additionally, Swami and Chandra (1987) proposed a pressure coefficient correlation based on wind direction and building dimensions. Two additional pressure coefficients were obtained through CFD: one without any barriers (CFD-Isolated) and another considering a building in a surrounding area with a plan density of 0.2 (CFD-Non-isolated). These coefficients reflect the influence of the surrounding environment on the building's airflow patterns.

Table 1: Scenarios of study

Case	Description
No wind	No wind action ($C_p = 0$)
EN15242	EN15242 pressure coefficient profile
Swami and Chandra (1987)	Literature correlation of Swami and Chandra (1987)
CFD-Isolated	CFD pressure coefficient profile for a building without any barrier surrounding
CFD-Non-isolated	CFD pressure coefficient profile for a building with a plan density area of 0.2

3 RESULTS AND DISCUSSION

3.1 Wall-averaged wind pressure coefficient

The wall-averaged wind pressure coefficient for low-rise buildings is presented in Figure 3 in which the relative surface angle (α) is defined as:

$$\alpha = \alpha_{\text{wind}} + \alpha_{\text{surface}} \tag{4}$$

where α_{wind} is the wind direction and α_{surface} is the wall orientation.

Figure 3: Wall-averaged wind pressure coefficient

(a) Isolated building.

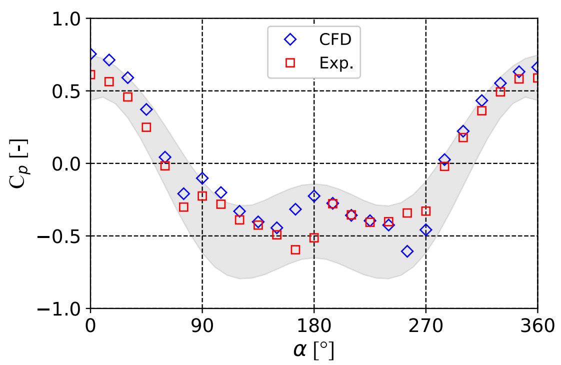

(b) Non-isolated building.

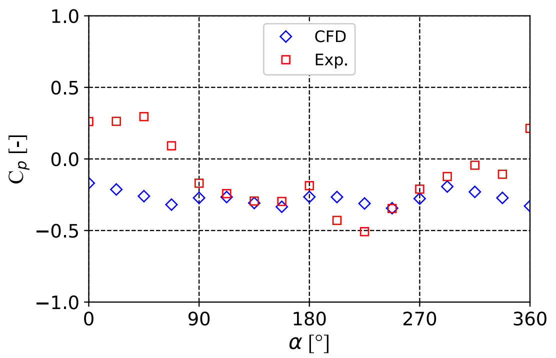

Regarding the isolated building (Figure 3a), besides the experimental data (“TPU Aerodynamic Database”, 2023) the CFD results were compared against the ASHRAE data range for low-rise buildings (ASHRAE, 2021) in which 80% of pressure coefficients are expected (the grey zone in the curve). The CFD results agreed quite well with the mean values from experimental data with higher errors in façade orientation of 90° (90° $\leq \alpha \leq$ 180°) and 180° (180° $\leq \alpha \leq$ 270°) with higher errors for relative surface angle near 180° and 270° (the relative error in this region is the order of 40%). These errors occurred due to the difficulty of CFD using RANS models to solve turbulence structures such as in flow separation regions and the vortices found in airflow around bluff bodies. However, almost 85% of points yielded errors as lower as 10% and the sign was the same leading to accurate pressure coefficient profiles using this CFD method for isolated low-rise buildings.

The airflow around buildings becomes even more complex when we have a neighbourhood. A building surrounded by buildings of similar height will have quite different airflow partners, i.e., different near-wall velocities and pressures. Consequently, the pressure coefficient will change and due to the large possibilities of surrounding patterns, there are fewer data found in the literature. Taking regular surroundings such as shown in Figure 1b will lead to the pressure coefficient profiles in Figure 3b. For façade orientation between 90° ($90° \leq \alpha \leq 180°$) and 270° ($270° \leq \alpha \leq 360°$), the errors were lowered, and the pressure coefficient profile was quite accurate. The CFD method of this study failed for the surface direction of 0° ($0° \leq \alpha \leq 90°$) mostly because for relative surface angle up to 70° the mean experiments are positive while CFD was negative. This difference in the sign is critical for natural ventilation analysis, therefore the CFD results must be improved in this façade.

3.2 IAQ in the modified BESTEST MZ320

The ACH for the whole building in Figure 2 is shown in Figure 4 in which each case was described in Table 1. When the wind action is neglected, we have ~1/3ACH for the whole building once we have an extract ventilation of 1ACH only in Zone C. Overall, when we consider the wind action the air change rate of the whole building is around 7% higher than no wind action.

Figure 4: Air change rate (whole building)

(a) Total simulation period. (b) Simulation between the second and fourth days.

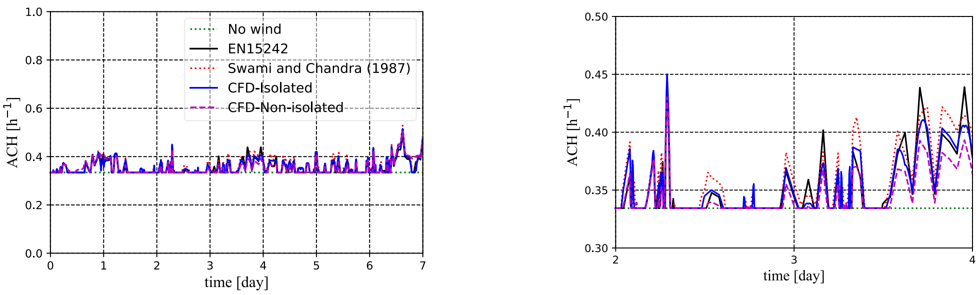

The only contaminant in this study was the CO_2 which is associated with the air change rate and is the most comment monitored building contaminant when it is important to control the building ventilation. The CO_2 concentration in Zone B is shown in Figure 5. As expected, improving the ventilation with mixed ventilation led to a reduction of the CO_2 concentration in the order of 6% for Zone B.

Figure 5: CO_2 concentration (Zone B)

(a) Total simulation period. (b) Simulation between the second and fourth days.

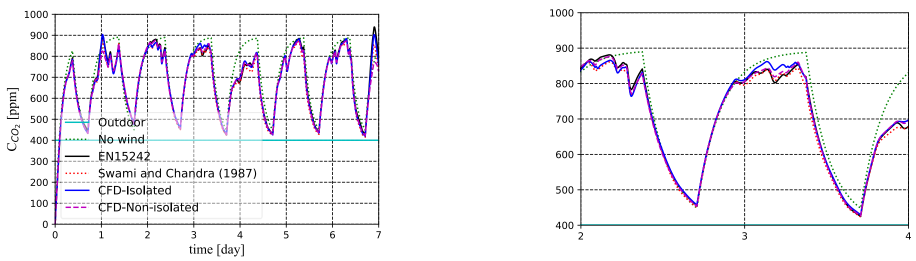

Table 2 sums up the IAQ indicators of this study in which the relative error (Er) is calculated against the case with “No wind”. The air change rate for the whole building is almost the same for the different forms to consider the pressure coefficient, therefore, for this case, there is no need to apply the CFD to obtain a pressure coefficient profile once we have almost the same outcomes regarding the straightforward correlations from the literature. Similar results were achieved for the decrease of the CO_2 concentration in Zone B and C, with lower concentrations in Zone B. In Zone A we observed a very large increase in the CO_2 due to when there is no wind, the outdoor contaminant concentration will not affect this zone. In addition, it is expected lower ventilation rates in Zone A for this building.

Table 2: Arithmetic mean of ACH (whole building) and median of CO_2 concentration

Case	ACH	Er_{ACH}	$\bar{C}_{CO_2}^{Zone\ A}$	$Er_{\bar{C}_{CO_2}}^{Zone\ A}$	$\bar{C}_{CO_2}^{Zone\ B}$	$Er_{\bar{C}_{CO_2}}^{Zone\ B}$	$\bar{C}_{CO_2}^{Zone\ C}$	$Er_{\bar{C}_{CO_2}}^{Zone\ C}$
No wind	0.334	-	59	-	754	-	497	-
EN15242	0.354	+6%	411	+599%	713	-6%	480	-3%
Swami and Chandra (1987)	0.360	+8%	409	+596%	703	-7%	476	-4%
CFD-Isolated	0.357	+7%	412	+602%	708	-6%	478	-4%
CFD-Non-isolated	0.354	+6%	411	+599%	708	-6%	482	-3%

4 CONCLUSIONS

This study performed numerical simulations employing the CFD method to obtain pressure coefficient profiles. These profiles were subsequently tested in the modified BESTEST MZ320 and compared against correlations found in the literature, as well as a case without wind effects.

To begin with, the CFD code was validated for low-rise buildings. It yielded errors as low as 10% for a building without barriers, although certain areas exhibited slightly higher errors for a building with a canyon street aspect ratio of 1.0 due to limitations in the RANS modeling technique.

Next, four pressure coefficient profiles were tested in the BESTEST MZ320 and compared with a case where no wind load was applied. This comparison focused on air change rates for the entire building and CO_2 concentrations in different zones. The results indicated an increase in the ACH of up to 8% and a decrease in CO_2 concentrations in two zones by as much as 7%.

While CFD may not be essential for this simple case, its significance is expected to be more pronounced in complex building scenarios. Therefore, future research should emphasize the importance of obtaining accurate profiles for pressure coefficients, include other IAQ indicators, explore additional scenarios such as cosimulation with BES software for non-isothermal conditions, and propose ventilation control strategies based on the most accurate boundary conditions attainable.

5 ACKNOWLEDGEMENTS

The authors would like to thank the Brazilian agency CAPES (Coordination of Superior Level Staff Improvement), of the Ministry of Education, for the financial support, the Binational Cooperation Program CAPES/COFECUB (Grant # 898/18), in collaboration with the laboratory LOCIE at the Université Savoie Mont-Blanc, France, and the Brazilian Research Council (CNPq) of the Ministry of Science, Technology and Innovation.

6 REFERENCES

Argyropoulos, C. D., A. M. Ashraf, L. Vechot, and K. E. Kakosimos. 2017. “Coupling Multi-Zone and CFD Models for Investigating Indoor Air Quality.” In Second International Conference on Energy and Indoor Environment for Hot Climates by ASHRAE. Doha, Qatar.

ASHRAE. 2021. ASHRAE HANDBOOK: Fundamentals, SI Edition. SI ed. American Society of Heating, Refrigeration and Air-Conditioning Engineers.

Beausoleil-Morrison, Ian. 2021. Fundamentals of Building Performance Simulation. Taylor & Francis.

Blocken, Bert. 2015. “Computational Fluid Dynamics for Urban Physics: Importance, Scales, Possibilities, Limitations and Ten Tips and Tricks towards Accurate and Reliable Simulations.” Building and Environment, Fifty Year Anniversary for Building and Environment, 91 (September): 219–245.

Dols, W. Stuart, and Brian J. Polidoro. 2020. CONTAM User Guide and Program Documentation Version 3.4. NIST Technical Note 1887. NIST.

Ferziger, Joel H., Milovan Pric, and Robert L. Street. 2020. Computational Methods for Fluid Dynamics. 4th ed. Springer.

Kato, Shinsuke. 2018. “Review of Airflow and Transport Analysis in Building Using CFD and Network Model.” JAPAN ARCHITECTURAL REVIEW 1 (3): 299–309.

Launder, B. E., and D. B. Spalding. 1974. “The Numerical Computation of Turbulent Flows.” Computer Methods in Applied Mechanics and Engineering 3 (2): 269–289.

Neymark, J., and R. Judkoff. 2008. International Energy Agency Building Energy Simulation Test and Diagnostic Method (IEA BESTEST). Multi-Zone Non-Airflow In-Depth Diagnostic Cases: MZ320 – MZ360. NREL/TP-550-43827.

Nikolaou, Andreas, and Michalis P. Michaelides. 2016. “CFD Simulation of Contaminant Transportation in High-Risk Buildings Using CONTAM.” In Critical Information Infrastructures Security, edited by Christos G. Panayiotou, Georgios Ellinas, Elias Kyriakides, and Marios M. Polycarpou, 135–146. Lecture Notes in Computer Science. Cham: Springer International Publishing.

Oke, Timothy R., Gerald Mills, Andreas Christen, and James A. Voogt. 2017. Urban Climates. Cambridge University Press.

Patankar, Suhas V. 1980. Numerical Heat Transfer and Fluid Flow. New York: McGraw-Hill Book Company.

Picozzi, Vincenzo, Antonio Malasomma, Alberto Maria Avossa, and Francesco Ricciardelli. 2022. “The Relationship between Wind Pressure and Pressure Coefficients for the Definition of Wind Loads on Buildings.” Buildings 12 (2). Multidisciplinary Digital Publishing Institute: 225.

Poirier, Baptiste. 2023. “Évaluation de La Performance Globale de La Ventilation Intelligente En Logement Basse Consommation.” PhD thesis. Le Bourget-du-Lac: Université Savoie Mont Blanc.

Poirier, Baptiste, Gaëlle Guyot, Monika Woloszyn, Hugo Geoffroy, Michel Ondarts, and Evelyne Gonze. 2021. “Development of an Assessment Methodology for IAQ Ventilation Performance in Residential Buildings: An Investigation of Relevant Performance Indicators.” Journal of Building Engineering 43: 103140.

Shu, Chang, Liangzhu (Leon) Wang, and Mohammad Mortezazadeh. 2020. “Dimensional Analysis of Reynolds Independence and Regional Critical Reynolds Numbers for Urban Aerodynamics.” Journal of Wind Engineering and Industrial Aerodynamics 203: 104232.

Singh, Manan, and Ryan Sharston. 2021. “A Literature Review of Building Energy Simulation and Computational Fluid Dynamics Co-Simulation Strategies and Its

Implications on the Accuracy of Energy Predictions." Building Services Engineering Research and Technology 43 (1). SAGE Publications Ltd STM: 113–138.
Swami, Muthusamy V., and Subrato Chandra. 1987. Procedures for Calculating Natural Ventilation Airflow Rates in Buildings. FSEC-CR-163-86. Florida: Florida Solar Energy Center.
Szczepanik-Scislo, Nina. 2022. "Improving Household Safety via a Dynamic Air Terminal Device in Order to Decrease Carbon Monoxide Migration from a Gas Furnace." International Journal of Environmental Research and Public Health 19 (3): 1676.
"TPU Aerodynamic Database." 2023. Accessed June 27. http://www.wind.arch.t-kougei.ac.jp/system/eng/contents/code/tpu.
Wang, Liangzhu. 2007. "Coupling of Multizone and CFD Programs for Building Airflow and Contaminant Transport Simulations." West Lafayette: Purdue University.
Wang, Liangzhu, Steven Emmerich, and Ryan Powell. 2010. Modeling the Effects of Outdoor Gasoline Powered Generator Use on Indoor Carbon Monoxide Exposures Phase II.
Wang, Liangzhu Leon, W. Stuart Dols, and Qingyan Chen. 2010. "Using CFD Capabilities of CONTAM 3.0 for Simulating Airflow and Contaminant Transport in and around Buildings." HVAC&R Research 16 (6): 749–763.
Wilcox. 2006. Turbulence Modeling for CFD. 3rd ed. DCW Industries.